Experimental evidence of zero-angle refraction and acoustic wave-phase control in a two-dimensional solid/solid phononic crystal

J. O. Vasseur,[1] B. Morvan,[2] A. Tinel,[2] N. Swinteck,[3] A.-C. Hladky-Hennion,[1] and P. A. Deymier[3]

[1]*Institut d'Electronique, de Microélectronique et de Nanotechnologie (IEMN, UMR CNRS 8520), 59652 Villeneuve d'Ascq, France*

[2]*Laboratoire Ondes et Milieux Complexes, UMR CNRS 6294, Université du Havre, 76610 Le Havre, France*

[3]*Department of Materials Science and Engineering, University of Arizona, Tucson, Arizona 85721, USA*

(Received 3 August 2012; revised manuscript received 5 October 2012; published 18 October 2012)

The square symmetry of the equifrequency contour of longitudinal waves in a solid/solid two-dimensional phononic crystal (PC) is shown through numerical calculations and experiments to lead to peculiar propagation phenomena. A slab of steel/epoxy PC immersed in water refracts incident longitudinal waves by an angle of zero degrees. The waves propagate along the shortest path between the slab faces. This characteristic enables the superposition within the same volume of the PC of waves with different incidence angles. Two incident waves with symmetrical incident angles can interfere constructively or destructively inside the PC depending on their initial phase difference. This phase difference is shown to enable control of wave propagation through the PC.

DOI: 10.1103/PhysRevB.86.134305 PACS number(s): 43.20.+g, 43.35.+d, 63.20.−e

I. INTRODUCTION

The field of phononic crystals (PCs) emerged over the past two decades. These materials are composite structures designed to tailor elastic wave dispersion (i.e., band structure) through Bragg scattering to achieve a range of spectral (ω-space), wave-vector ($\vec{k}$-space), and wave-phase (φ-space) properties. The periodic nature of PCs may introduce band gaps in the transmission spectrum of these artificial materials whereby the propagation of elastic waves is forbidden in some interval of frequency.[1–4] Spectral properties of PCs have been studied over extensive frequency ranges, from the sonic audible range to the ultrasonic range (kHz-MHz) to hypersonic frequencies (GHz).[5–7] Wave localization phenomena in defected PCs containing linear and point defects have also been considered.[8–10] Here, the properties of the defected PCs arise from defect modes localized within spectral gaps of the PC. The wave-vector ($\vec{k}$-space) properties of PCs result from passing bands with unique refractive characteristics, such as negative refraction or zero-angle refraction. Negative refraction of acoustic waves is analogous to negative refraction of electromagnetic waves also observed in photonic crystals[11] and electromagnetic metamaterials.[12] In PCs, negative refraction is achieved through band-folding effect via Bragg scattering. Band folding can produce bands with negative slope (i.e., negative group velocity and positive phase velocity), a prerequisite for negative refraction. A combined theoretical and experimental study of a three-dimensional PC composed of tungsten carbide beads in water has shown the existence of a strongly anisotropic band with negative refraction.[13] A two-dimensional PC constituted of a triangular lattice of steel rods immersed in a liquid exhibited negative refraction and was used to focus ultrasound.[14,15] High fidelity imaging is obtained when all-angle negative refraction conditions are satisfied; that is, the equifrequency contour (EFC) of the PC is circular and matches that of the medium in which it is embedded. A flat lens of this latter crystal achieved focusing and subwavelength imaging of acoustic waves[16] by transmitting the evanescent components of a sound point source via the excitation of a vibrational mode bound to the PC slab. A broader range of unusual refractive properties was also reported in a study of a PC consisting of a square array of cylindrical polyvinylchloride inclusions in air.[17] This crystal exhibited positive, negative, or zero refraction depending on the angle of the incident sound beam. Zero-angle refraction can lead to wave guiding/localization without defects.[18–21] Only recently, has progress been made in the extension of properties of PCs beyond ω and $\vec{k}$ spaces and into the realm of acoustic wave-phase space (φ space).[22–24] The concept of phase control between propagating waves in a PC can be realized through analysis of its band structure and EFC.[22] The dominant mechanisms behind the control of phase between propagating acoustic waves in two-dimensional PCs arises from the anisotropy of the EFC resulting in the noncollinearity of the wave and group velocity vectors. In this situation, the relative phase between incident waves impinging on a finite PC can be precisely modulated by either changing the incident angles of the incoming acoustic beams (i.e., changing the phase velocity at which the beams travel in the PC) or varying the thickness of the PC. Impinging beams that have different incident angles, but excite the same Bloch modes in the PC, referred to as complementary waves, travel the same path (i.e., the path consistent with the angle of refraction). Altering the relative phase between the incident beams changes the manner in which these modes superpose within the PC and can lead to constructive or destructive interferences subsequently affecting their transmission. In this paper, we built on the recent report of a two-dimensional solid/solid PC composed of steel cylindrical inclusions arranged on a square lattice and embedded in an epoxy matrix. This PC was shown previously to possess a passing band of longitudinal polarization with a nearly square EFC over a wide range of frequency (see Fig. 1).[25] When the PC is immersed in an appropriate medium (water), the anisotropy of this band can lead to zero-angle refraction over a wide range of incident angles. In addition, since the EFC of the incident homogeneous medium is larger than that of the PC in the first Brillouin zone (BZ), upon exiting the PC, the transmitted wave exhibits splitting. We verify the property of zero-angle refraction and beam splitting by a combination of wave-vector diagrams, finite difference time domain (FDTD) calculations and experiments.

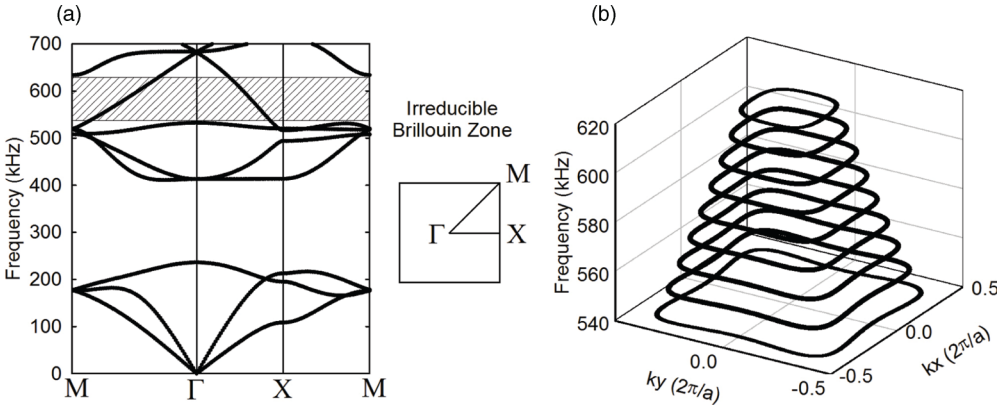

FIG. 1. (a) Band structure calculated with the plane wave expansion method (Refs. 2 and 3) of the infinite, periodic steel/epoxy PC (square array, lattice parameter $a = 3.23$ mm, filling factor $f = 30\%$) along high symmetry directions in the irreducible Brillouin zone. This band structure is limited to vibrational modes in the plane perpendicular to the inclusions. A large band gap is observed between 238 and 410 kHz. From 540 to 620 kHz (shaded region), a passing band with negative slope stands alone. (b) EFCs over frequency range 540–620 kHz [shaded region in (a)]. The squarelike shape of these contours allows for zero-angle refraction phenomena for a wide range of incidence angles of acoustic beams (after Ref. 25).

Furthermore, we demonstrate unambiguously the control of the wave-phase properties of this PC by showing that the transmission of two complementary waves can be modified by varying the relative phase of the incident waves that can interfere constructively (transmission) or destructively (no transmission). In Sec. II, we present the experimental setups used to show (a) zero-angle refraction and splitting of the acoustic beam transmitted through the steel/epoxy PC and (b) zero-angle refraction and the excitation of Bloch modes by two complementary incident beams. The results reported in Sec. III demonstrate zero-angle refraction and the control of interference of refracted complementary acoustic waves within the volume of the PC. In Sec. IV, we conclude as to the applicability of PC with distinctive phase properties to broaden the field of phononics-based technologies.

II. METHODS

A. Experimental setups

1. Sample

The sample of steel/epoxy PC is constituted of an array of 240 parallel cylinders of steel arranged on a square lattice and embedded in an epoxy resin matrix. The metallic cylinders have a radius $R = 1$ mm and the periodicity of the square lattice is $a = 3.23$ mm. Subsequently, the filling fraction of metal to resin, defined as the ratio between the cross-sectional area of one rod and the surface of one unit cell, is equal to 0.30. The sample was prepared as follows. A cubic mould, 15 cm × 4 cm × 10 cm, was fabricated by assembling five Plexiglas plates. 2-mm-diameter × 5-mm-deep bores, arranged on square array, were drilled on two opposite sides of the mould to maintain the metal cylinders. Clean steel cylinders were then placed and fixed between these two plates. The liquid epoxy resin was poured in the mold and degassed during a long period of time to ensure that most of the trapped air was evacuated. After hardening, the composite material was removed from the mold and the faces of the specimen were pumiced and polished in order to obtain surfaces as smooth as possible. At the end of the sample preparation, the physical dimensions of the specimen were 13.2 cm × 2 cm × 10 cm with 40 and 6 rows of cylinders along the width and the thickness of the sample, respectively.

2. Setup for zero-angle refraction and beam splitting

To characterize experimentally the transmission and the refractive properties of the PC, we use a single 1.5 in. immersion source transducer (broadband centered on 500 kHz) with variable position and orientation with respect to the sample. All distances d and d' (see Fig. 2) will be chosen larger than several wavelengths to ensure the far-field assumption. The detection transducer is mounted on a motorized stage that can produce a raster of the acoustic field on the exit side of the PC along the vertical direction. The source signal is emitted with an Agilent generator as a burst of sinusoids of duration equal to ten periods with a peak-to-peak amplitude of 10 V. Using bursts enables us

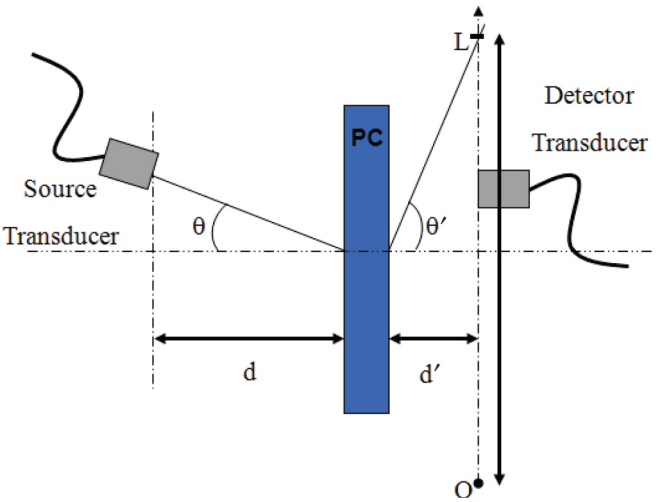

FIG. 2. (Color online) Experimental setup with single source (540 kHz) and scanning motorized detector. The entire setup is immersed in water.

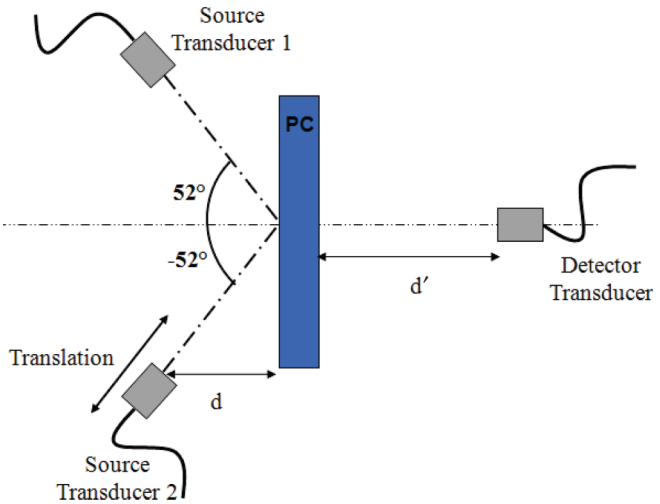

FIG. 3. (Color online) Experimental setup with dual source (540 kHz) and scanning motorized detector. The entire setup is immersed in water. The relative phase between signals emitted by sources 1 and 2 is controlled through a translation of the second source transducer.

to unravel the spatiotemporal response of the water|PC|water system. The operation frequency was chosen as 540 kHz. At this frequency, we observed experimentally transmitted beams with the strongest intensity and the lowest spatial dispersion. These conditions are indicative of PC EFC with square shape and nearly flat faces. The transmitted signal is analyzed with a Yokogawa oscilloscope. All temporal signals are averaged over 128 data acquisitions. Data are reported in the time-space domain but also in the frequency-wave number domain through a fast Fourier transform (FFT).

3. Setup for acoustic wave-phase control

In this setup (see Fig. 3), we use two sources with identical characteristics (1.5 in. immersion source transducer, broadband centered on 500 kHz) oriented at $+52^\circ$ and -52° in order to excite equivalent Bloch modes inside the PC. Both transducers emit signals generated by the same Agilent generator. The signal takes the form of bursts of sinusoids of duration equal to 100 periods with a peak-to-peak amplitude of 10 V. We control the phase difference between the two input signals by translating one of the transducers by increments of 0.1 mm. At an operation frequency of 540 kHz, i.e., a wavelength in water of 2.78 mm, each increment in translation corresponds to a phase shift of 13°. The temporal data is calculated as an average of 60 acquisitions.

B. Model and computational method

Simulations of acoustic waves impinging upon a finite PC immersed in water, are performed with the FDTD method.[25–30] The geometrical characteristics of the modeled PC are identical to those of the experimental sample. In the FDTD method, the elastic wave equation is discretized in time and space on a square grid. For each source on the input side of the simulation space, we have a slanted line of grid points consistent with the desired incidence angle of the source. The nodes along this line are displaced in a direction orthogonal to the source line sinusoidally in time. At each time step, from spatial derivatives, the divergence of the stress tensor is calculated, which allows for the iterative update of the displacement field. Simulations are run for 2^{18} time steps with time step $\Delta t = 1.96 \times 10^{-9}$ s and spatial discretizations $\Delta x = \Delta y = a/50$. These parameters are chosen to ensure convergence of the numerical method. To close the simulation space in the x and y directions, first-order Mur absorbing boundary conditions are employed to avoid reflections and spurious simulation artifacts.[31] The density, longitudinal, and transverse velocities of sound for steel, epoxy, and water are listed in Table I. These parameters are obtained from the literature and may deviate slightly from the actual values of the materials used in the experiments. We anticipate slight discrepancies in the spectral response of the simulated system compared to that of the experimental crystal. For all simulations we chose an operation frequency of 590 kHz which corresponds to nearly square EFC with the flattest faces. The choice of this condition for the numerical simulations provides the best comparison with the experimental data. The properties of the simulated water|PC|water system are characterized subsequently by spatial maps of instantaneous pressure field.[25]

TABLE I. Density, longitudinal speed of sound, and transverse speed of sound for steel, epoxy, and water.

Material	Density ($\mathrm{kg\,m^{-3}}$)	Longitudinal velocity of sound ($\mathrm{m\,s^{-1}}$)	Transverse velocity of sound ($\mathrm{m\,s^{-1}}$)
Steel	7780	5825	3227
Epoxy	1180	2535	1157
Water	1000	1500	

III. RESULTS AND DISCUSSION

A. Zero-angle refraction and beam splitting

1. Normal incidence

To demonstrate the transmission and refraction properties of the steel/epoxy PC, we utilize first a wave-vector diagram [see Fig. 4(a)] and FDTD simulations [see Fig. 4(b)]. A slab of the steel/epoxy PC is sandwiched between two regions filled with water, an entrance region, and an exit region. Pictured in the center of Fig. 4(a) is an extended zone scheme representation of the PC's first BZ with squarelike EFCs corresponding to 590 kHz waves. The irreducible BZ (ΓXM) matches that shown in Fig. 1(a). On the left and the right of the PC, we see circular EFCs of radius $k = \omega/c_{\mathrm{water}}$, where c_{water} is the speed of longitudinal acoustic waves in water. At the interface between the entrance (respectively, exit) medium and the input (respectively, output) side of the PC, conservation of the component of the wave vector $\vec{k}$ parallel to the interface needs to be satisfied. A normal incident wave (OA) excites Bloch mode F inside the first BZ. Incident waves at $+52^\circ$ angle (OA′) or at -52° angle (OA″) excite the Bloch modes in the second and third BZ, E and G, respectively. An incident angle of $+52^\circ$ corresponds to the situation where the horizontal line A'E [which illustrates the conservation of the parallel component of the wave vector at the water/PC input side

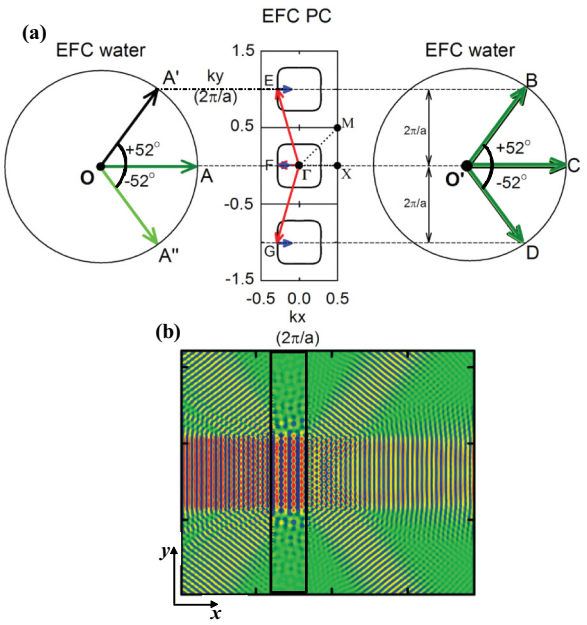

FIG. 4. (Color online) (a) (Center) An extended zone scheme representation of the first BZ for the epoxy/steel PC. EFCs are shown at 590 kHz. To the left and the right are circular contours representing longitudinal waves in water (see text for details). (b) Pressure field in a water|PC|water system calculated with the FDTD method. The source emits wave normal to the entrance PC surface. Splitting of the transmitted wave into three beams is clearly seen on the exit side of the PC. Vertical lines indicate the entrance and the exit sides of the PC.

interface in Fig. 4(a)] intersects the flat side of the EFC exactly in its middle. The value of this peculiar angle depends on the operation frequency, the speed of sound in water, and the lattice parameter. The normal incident wave also excites the modes E and G equivalent to mode F by translational symmetry of $2\pi/a$. The two impinging waves at $\pm 52^\circ$ are perfectly symmetric with respect to the horizontal axis and excite the same equivalent Bloch modes (referred to as E, F, and G) in the PC. Since the EFC of water is much larger than the EFC in the first BZ of the PC, the Bloch modes F, E, and G, upon exiting the PC, lead to three transmitted split beams at 0° and $\pm 52^\circ$ with respect to the normal of the PC surface. These split beams are represented by arrows O'B, O'C, and O'D in Fig. 4(a). Inside the PC, the modes F, E, and G have a group velocity normal to the vertical faces of the EFC, and elastic energy propagates in that same direction irrespective of the incident wave. This is characteristic of zero-angle refraction phenomena.[17–19] Figure 4(b) shows the pressure field calculated by FDTD in the case of a normal incident acoustic wave impinging upon the PC. The pressure field on the exit side of the PC clearly shows beam splitting that is a normal exit beam and two beams propagating at $\pm 52^\circ$. This behavior is verified experimentally using the setup of Fig. 2 with $d = 92$ mm and $d' = 50$ mm, $\theta = 0^\circ$ and θ' varying between -67.38° and 67.38°. This corresponds to a scan of 240 mm by the detector transducer. The spatial resolution of the scan is 1 mm. Figure 5(a) illustrates the amplitude of the spatiotemporal signal recorded at the exit side of the PC. This figure shows a strong transmitted beam propagating in the direction parallel to the normal of the PC surface as well as two weaker symmetrical beams represented by dotted squares. Fourier transform of the spatiotemporal field leads to a wave number/frequency diagram reported in Fig. 5(b) where the three high-amplitude spots correspond to the three transmitted

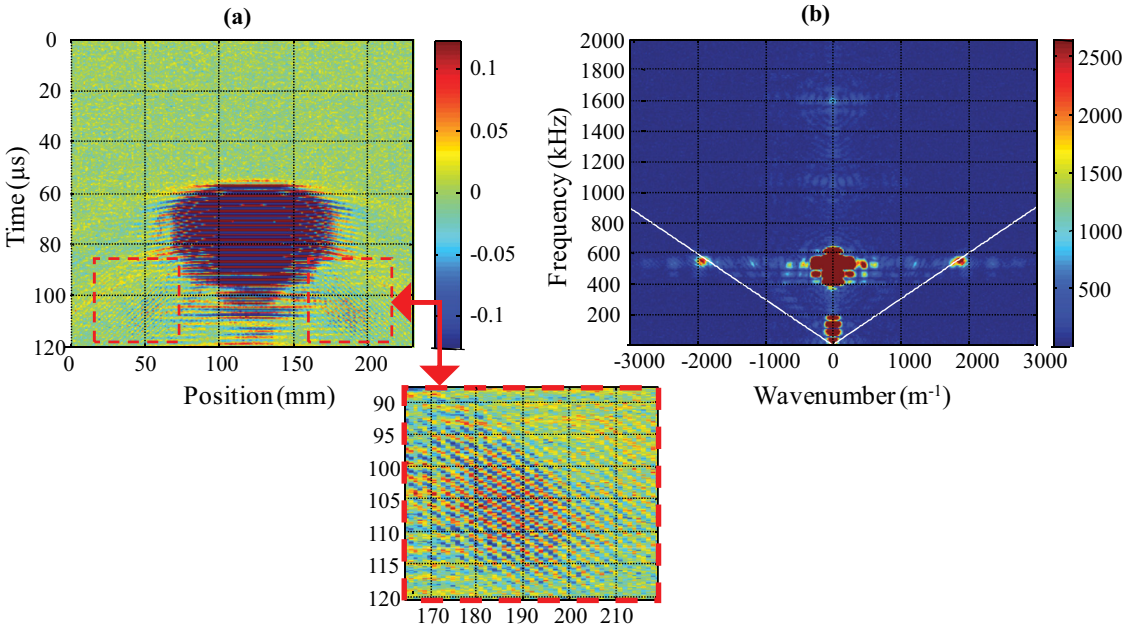

FIG. 5. (Color online) (a) Amplitude (in arbitrary units) of the experimental spatiotemporal response of the detector transducer for a source emitting at 540 kHz and at normal incidence. The horizontal axis corresponds to positions of the detector parallel to the exit surface of the PC at a distance of 90 mm. Red squares indicate two symmetrical waves that go out obliquely from the PC. The right red square is enlarged in the inset. (b) FFT (in arbitrary units) of the spatiotemporal response. The two white lines correspond to the projection of the wave number in water at angles θ' respectively equal to -52° and 52° with respect to the direction parallel to the exit surface of the PC.

split beams at 0° and ±52° with respect to the normal of the PC surface. The experimental results are in very good quantitative agreement with the FDTD calculations.

2. *Oblique incidence*

In this section, we focus on demonstrating experimentally the phenomenon of zero-angle refraction. For this, we again use the setup of Fig. 2 with $d' = 90$ mm, $\theta' = 0°$, $\theta = 52°$, and $d = 31$ mm (line of sight distances between emitting transducer and PC of 50 mm). Following the discussion of the wave-vector diagram of Fig. 4(a), an incident beam of 52° angle will be refracted at the PC surface with an angle of 0°, and will propagate inside the PC along the normal to the surface. Again upon exit three waves will be transmitted at the angles of 0° and ±52°. Observation of the transmitted beam at an angle near 0°, together with the FDTD calculations, will therefore be the signature of zero-angle refraction at the entrance of the PC. For this we limit the vertical scan of the detector to a narrower line segment of 100 mm. The spatiotemporal response of the detector along with its Fourier transform, are shown in Fig. 6. The single and intense spot in the (wave number, frequency) diagram almost centered on $k = 0$ indicates unambiguously the presence of a nearly normal exit beam and therefore of zero-angle refraction.

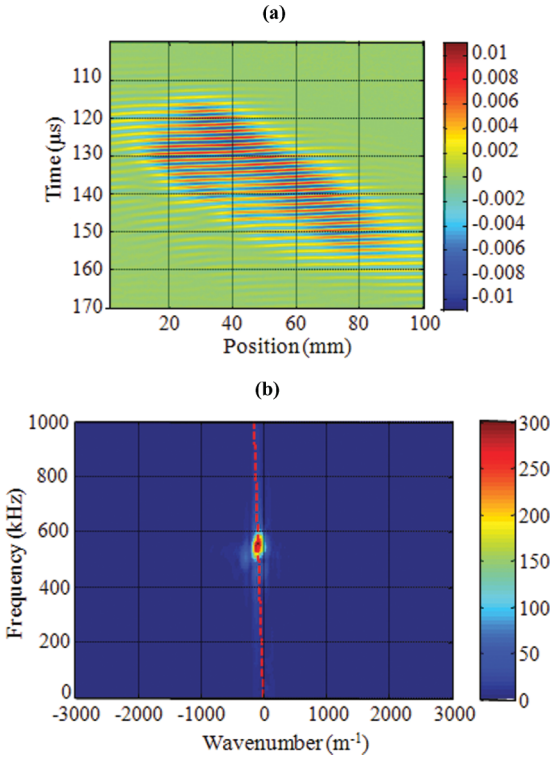

FIG. 6. (Color online) (a) Amplitude (in arbitrary units) of the spatiotemporal response of the detector transducer for an incident wave with an angle of 52° with respect to the PC input surface. The horizontal axis corresponds to positions of the detector parallel to the exit surface of the PC at a distance of 90 mm. The apparent spreading of the exit beam from, approximately, 10 to 90 mm is a consequence of the finite width of the oblique incident beam. (b) FFT (in arbitrary units) of the spatiotemporal response.

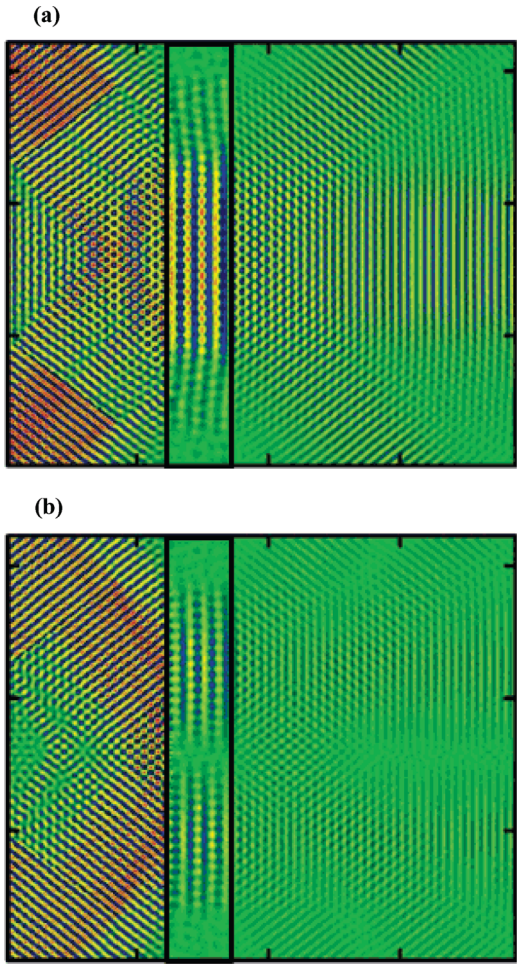

FIG. 7. (Color online) (a) and (b) FDTD simulation [instantaneous pressure field (P)]. Vertical lines indicate the entrance and the exit sides of the PC. Two acoustic waves (complementary angle inputs) in water impinge upon the PC surface at +52° and −52°. In (a), the acoustic sources oscillate in phase and excite identical Bloch modes in the PC k space. Bloch wave amplitudes constructively interfere inside the PC and highly intense, collimated acoustic energy is observed inside the PC. On the backside of the PC, beam splitting is observed. The three exiting beams are intense due to constructive wave interference. In (b), the acoustic sources oscillate π radians out of phase. Wave amplitudes destructively interfere inside the PC, resulting in a near-zero pressure field on the backside of the crystal.

B. Zero-angle refraction and phase control

In this section, we utilize the steel/epoxy PC as a phase-control device for manipulating acoustic wave propagation. For this we consider the interferences between two complementary incident beams as a function of their relative phase. In Fig. 7(a), an FDTD simulation mapping instantaneous pressure (P), shows the two complementary angle inputs. The acoustic sources are angled at +52° and −52°. These sources oscillate in phase with each other and enter the PC at precisely the same location. We observe a region of intense pressure inside the PC that is indicative of zero-angle refraction and constructive interferences between the superposed signals. Upon exiting the crystal, we see beam splitting. If the relative phase between the complementary beams is adjusted such

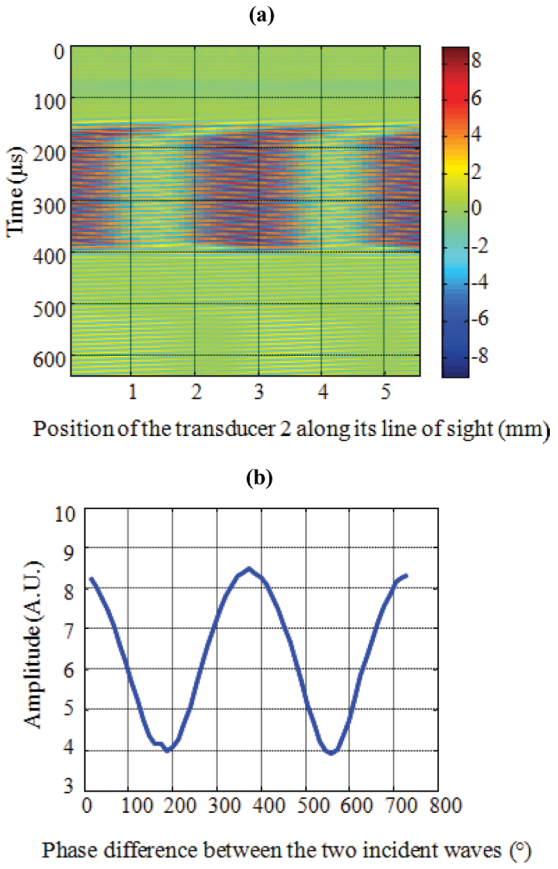

FIG. 8. (Color online) (a) Amplitude (in arbitrary units) of the temporal response of a fixed detector transducer on the exit side of the PC subjected to two acoustic beams. The angles of the two incident beams are $\pm 52^{\circ}$. The horizontal axis corresponds to the position of the second source along its line of sight. (b) Response of the detection transducer as a function of the phase difference between the two incident beams. Maxima (resppectively, minima) occur for phase difference equal to an even (respectively, odd) multiple of $180^{\circ} = \pi$ rad.

that the sources oscillate π radians out of phase [Fig. 7(b)], then destructive interferences occur between propagating equivalent Bloch modes inside the PC and opposing wave amplitudes annihilate each other to yield a near-zero pressure field on the backside of the PC. We have shown theoretically[25] that maxima of pressure for in-phase sources and minima for out-phase sources are much more contrasted when considering a thicker PC sample. Behaviors reported in Figs. 7(a) and 7(b) are confirmed experimentally in Fig. 8. The experimental setup described in Fig. 3 is applicable hereafter. Figure 8(a) shows the amplitude of the temporal response of the fixed detector as a function of the position of the second source along its line of sight. The presence of bands alternating in amplitude demonstrates maxima of transmission for this position equals multiples of the wavelength ($\lambda = 2.73$ mm) and minima of transmission for the same position equals odd multiples of half the wavelength. This results from constructive or destructive interferences between the Bloch modes that superpose spatially inside the PC. This spatial superposition is made possible by the zero-angle refraction of the two complementary incident beams. In Fig. 8(b), the evolution of the detected transmitted amplitude is plotted as a function of the phase difference between the two incident complementary waves. Maxima of amplitude occur when the waves are in phase and amplitude is minimal when the sources oscillate out of phase. The figure does not show complete extinction. This is probably due, on one hand, to structural and operational differences between the two input transducers. On the other hand, complete extinction of the output signal should be facilitated by using thicker samples,[25] however, epoxy is a rather strongly absorbing medium and attenuation in this material requires the use of relatively thin samples. Nevertheless, experimental results are in excellent agreement with the numerical predictions and demonstrate the possibility of using PCs to control propagation of acoustic waves through phase modulation.

IV. CONCLUSION AND PERSPECTIVES

Following the discovery of a two-dimensional solid/solid PC with quasisquare EFC for longitudinal waves,[25] we demonstrate numerically and experimentally its properties of zero-angle refraction and acoustic waves transmission through phase control. A finite-size PC composed of steel inclusions in epoxy is immersed in water and shown (a) to refract incident waves with an angle of zero degrees over a wide range of incident angles, (b) to support multiple equivalent Bloch modes that propagate collinearly, and (c) to mix complementary incident waves inside the same volume of the PC allowing constructive or destructive interferences depending on their relative phase. This φ-space function is wholly enabled by the symmetry of the EFC. This is the first ever experimental demonstration of phase control between propagating acoustic waves within a solid/solid PC. The function demonstrated in this paper can be interpreted as a NOT logic gate. For instance, encoding the input binary numbers 0 and 1 in the phase difference between the two incident beams ($\Delta\varphi = 0$ and π) results in high and low transmitted amplitude that could encode the output binary numbers 1 and 0. Other Boolean logic gates based on phase control in PCs have been demonstrated numerically.[24] The present paper proves the possibility of their experimental realization.

ACKNOWLEDGMENTS

We gratefully acknowledge support from National Science Foundation Grant No. 0924103. J.O.V and A.C.H.H. acknowledge partial support from Centre National de la Recherche Scientifique (CNRS) through Laboratoire International Associé (LIA) "MATEO" with the University of Arizona.

[1]M. M. Sigalas and E. N. Economou, J. Sound Vib. **158**, 377 (1992).

[2]M. M. Sigalas and E. N. Economou, Solid State Commun. **86**, 141 (1993).

[3]M. S. Kushwaha, P. Halevi, L. Dobrzynski, and B. Djafari-Rouhani, Phys. Rev. Lett. **71**, 2022 (1993).
[4]J. O. Vasseur, P. A. Deymier, B. Chenni, B. Djafari-Rouhani, L. Dobrzynski, and D. Prevost, Phys. Rev. Lett. **86**, 3012 (2001).
[5]T. Gorishnyy, C. K. Ullal, M. Maldovan, G. Fytas, and E. L. Thomas, Phys. Rev. Lett. **94**, 115501 (2005).
[6]T. Still, W. Cheng, M. Retsch, R. Sainidou, J. Wang, U. Jonas, N. Stefanou, and G. Fytas, Phys. Rev. Lett. **100**, 194301 (2008).
[7]D. Schneider, F. Liaqat, E. H. El Boudouti, Y. El Hassouani, B. Djafari-Rouhani, W. Tremel, H.-J. Butt, and G. Fytas, Nanoletters **12**, 3101 (2012).
[8]6. M. Torres, F. R. Montero de Espinosa, D. Garcia-Pablos, and N. Garcia, Phys. Rev. Lett. **82**, 3054 (1999).
[9]M. Kafesaki, M. M. Sigalas, and N. Garcia, Phys. Rev. Lett. **85**, 4044 (2000).
[10]A. Khelif, B. Djafari-Rouhani, J. O. Vasseur, P. A. Deymier, Ph. Lambin, and L. Dobrzynski, Phys. Rev. B **65**, 174308 (2002).
[11]J. B. Pendry, Phys. Rev. Lett. **85**, 3966 (2000).
[12]N. Engheta and R. W. Ziolkowski, *Metamaterials: Physics and Engineering Explorations* (Wiley, New York, 2006).
[13]S. Yang, J. H. Page, Z. Liu, M. L. Cowan, C. T. Chan, and P. Sheng, Phys. Rev. Lett. **93**, 024301 (2004).
[14]M. Ke, Z. Liu, C. Qiu, W. Wang, J. Shi, W. Wen, and P. Sheng, Phys. Rev. B **72**, 064306 (2005).
[15]A. Sukhovich, L. Jing, and J. H. Page, Phys. Rev. B **77**, 014301 (2008).
[16]A. Sukhovich, B. Merheb, K. Muralidharan, J. O. Vasseur, Y. Pennec, P. A. Deymier, and J. H. Page, Phys. Rev. Lett. **102**, 154301 (2009).
[17]J. Bucay, E. Roussel, J. O. Vasseur, P. A. Deymier, A-C. Hladky-Hennion, Y. Pennec, K. Muralidharan, B. Djafari-Rouhani, and B. Dubus, Phys. Rev. B **79**, 214305 (2009).
[18]I. Pérez-Arjona, V. J. Sanchez-Morcillo, J. Redondo, V. Espinosa, and K. Staliunas, Phys. Rev. B **75**, 014304 (2007).
[19]V. Espinosa, V. J. Sanchez-Morcillo, K. Staliunas, I. Perez-Arjona, and J. Redondo, Phys. Rev. B **76**, 140302(R) (2007).
[20]J. S. Shi, S. S. Lin, and T. J. Huang, Appl. Phys. Lett. **92**, 111901 (2008).
[21]W. Liu and X. Su, Phys. Lett. A **374**, 2968 (2010).
[22]N. Swinteck, J-F. Robillard, S. Bringuier, J. Bucay, K. Muralidharan, J. O. Vasseur, K. Runge, and P. A. Deymier, Appl. Phys. Lett. **98**, 103508 (2011).
[23]N. Swinteck, S. Bringuier, J.-F. Robillard, J. O. Vasseur, A. C. Hladky-Hennion, K. Runge, and P. A. Deymier, J. Appl. Phys. **110**, 074507 (2011).
[24]S. Bringuier, N. Swinteck, J. O. Vasseur, J.-F. Robillard, K. Runge, K. Muralidharan, and P. A. Deymier, J. Acoust. Soc. Am. **130**, 1919 (2011).
[25]N. Swinteck, J. O. Vasseur, A. C. Hladky-Hennion, C. Croenne, S. Bringuier, and P. A. Deymier, J. Appl. Phys. **112**, 024514 (2012).
[26]D. Garcia-Pablos, M. Sigalas, F. R. Montero de Espinosa, M. Torres, M. Kafesaki, and N. Garcia, Phys. Rev. Lett. **84**, 4349 (2000).
[27]T. Miyashita and C. Inoue, Jpn. J. Appl. Phys., Part 1 **40**, 3488 (2001).
[28]Ph. Lambin, A. Khelif, J. O. Vasseur, L. Dobrzynski, and B. Djafari-Rouhani, Phys. Rev. E **63**, 066605 (2001).
[29]M. Sigalas and N. Garcia, J. Appl. Phys. **87**, 3122 (2000).
[30]M. Torres, F. R. Montero de Espinosa, and J. L. Aragon, Phys. Rev. Lett. **86**, 4282 (2001).
[31]G. Mur, IEEE Trans. Electromagn. Compat. **EMC-23**, 377 (1981).